Classification of the Core Modes of Hollow-Core Photonic-Bandgap Fibers

Kiarash Zamani Aghaie, Vinayak Dangui, Michel J. F. Digonnet, Shanhui Fan, *Senior Member, IEEE*, and Gordon S. Kino, *Life Fellow, IEEE*

***Abstract*—Using a new full-vectorial finite-difference mode solver utilizing a hexagonal Yee's cell, we calculated the dispersion diagram of a slightly multimode (16 modes) air-core photonic-bandgap fiber (PBF) and the electric-field profiles of all of its core modes. Careful comparison shows striking similarities between these properties and those of the hybrid modes of a conventional step-index fiber, in terms of the modes' field profiles, the modes' degeneracy, the order in which the modes mode cut off in the wavelength space, and the maximum number of modes. Based on these similarities, we propose for the first time a systematic nomenclature for the modes of a PBF, namely hybrid HE and EH modes and of quasi-TE and quasi-TM modes. Other small but relevant similarities and differences between the modes of these two types of fibers are also discussed.**

***Index Terms*—Finite difference methods, optical fibers, optical fiber communication.**

I. Introduction

As a result of their much weaker optical nonlinearities [1], weaker sensitivity to temperature [2], [3], and higher resistance to optical damage, hollow-core photonic-bandgap fibers (PBF) are finding a wide range of potential applications, in particular for the delivery of high peak powers [4], for the generation of high-power solitons [5], for picosecond pulse compression [6], data transmission [7] and in fiber optic gyroscopes [3], [8]. Of the extensive literature on PBFs, a sizable fraction is devoted to elucidating and improving the fiber modal properties, especially understanding the impact of surface modes on their propagation loss and dispersion [9], widening their bandgap [10], and suppressing surface modes [11] and higher order modes [12]. However, it is surprising that no comprehensive study of the guided modes of these interesting fibers has been reported. To our knowledge, modal studies are limited to one article reporting the calculated vector fields of the second-order modes of a hollow-core fiber [12], as a sideline to a larger study. In another study, the calculated dispersion curves, confinement losses, and surface scattering coefficients of two multimoded hollow-core fibers are presented [13]. Yet many of the finer aspects of PBF modes that have not yet been investigated are critical to understand these intriguing fibers and to properly implement them in each of their many applications. Another consequence is that there is still no consensus for the names of the modes of these fibers. Different authors use different names to designate the same modes, which leads to confusion and possible misinterpretations. For example, the fundamental mode is indiscriminately referred to as HE_{11} [12], HE_{11}-like [14], LP_{01} [15], or even MP_{11} (for mixed polarization) in the particular subset of Bragg fibers [16]. The situation is even more confusing with higher order modes, which are identified by what we believe is their proper names (e.g., $\mathrm{TE}_{n,m}$ or $\mathrm{EH}_{n,m}$) only in one [12]. There is clearly a need to standardize this situation and provide a nomenclature for these modes.

The main purpose of this paper is to fill these gaps by providing a basic numerical description of the mode profiles and of a multimoded PBF and following through with a proposed nomenclature. Three years ago, we made headway in this direction by pointing out, via geometrical optics arguments, the strong analogies between the modal behavior of a PBF and that of a conventional index-guiding fiber, although at the time no attempt was made to investigate the symmetry and classify the core modes [17]. We refined the concept of V number for a PBF, and showed that at a particular frequency, the number of core modes supported by a PBF is essentially the same as that of an equivalent conventional (step-index) fiber with the same V number. In the present publication, we take this former study one step further and report the electric field and intensity profiles of all the core modes of a slightly multimoded PBF, calculated numerically using the latest generation of our photonic-bandgap mode simulator [18]. PBF modes are found to fall in two categories: hybrid modes, further subdivided in HE and EH modes, and quasi-transverse modes, further subdivided in quasi-TE and quasi-TM modes. As expected from symmetry considerations, the profiles of these modes are very similar to the profiles of the higher order modes of the equivalent conventional fiber. At a given frequency, the relative positions of the propagation constants of groups of modes in the dispersion diagram are found to be the same as for the equivalent conventional fiber. Based on these similarities, we propose to extend the analogy between a conventional fiber and a PBF developed in [17] and name all higher order modes the same way as in conventional fibers, as is already done for the second-order modes of hollow-core fibers [12], and for the core modes of solid-core microstructured fibers [19].

II. Symmetry Considerations

The core modes of conventional index-guiding fibers with cylindrical symmetry have well-known properties [20]. They

Manuscript received January 16, 2009; revised March 10, 2009. Current version published August 29, 2009. This work was supported by Litton Systems, Inc., a wholly owned subsidiary of Northrop Grumman Corporation.

The authors are with the Edward L. Ginzton Laboratory, Stanford University, Stanford, CA 94305 USA (e-mail: kzamani@stanford.edu; silurian@stanford.edu; shanhui@stanford.edu; kino@stanford.edu).

Color versions of one or more of the figures in this paper are available online at http://ieeexplore.ieee.org.

Digital Object Identifier 10.1109/JQE.2009.2019767

consist of doubly degenerate hybrid modes labeled $\mathrm{HE}_{m,n}$ and $\mathrm{EH}_{m,n}$, where $m \geq 1$ is the azimuthal number and n is the radial number, and non-degenerate transverse modes labeled $\mathrm{TE}_{0,n}$ and $\mathrm{TM}_{0,n}$. The latter are characterized by a null longitudinal field component, either E_z (TE modes) or H_z (TM modes), where z is the direction of propagation. Hybrid modes have all non-zero field components and exhibit either a larger E_z (HE modes) or a larger H_z (EH modes) component. There are two near-degeneracies in the modes' effective indices, namely for $\mathrm{HE}_{m,n}$ and $\mathrm{EH}_{m-2,n}$, and for $\mathrm{TE}_{0,n}$, $\mathrm{TM}_{0,n}$ and $\mathrm{HE}_{1,n}$.

When the refractive index difference between the fiber core and cladding is small enough (typically of $\sim$2% or less), or equivalently when the numerical aperture (NA) of the fiber is small, the modes are weakly guided, and under the well-known weakly guiding approximation the near-degeneracies mentioned above are approximated to be exact degeneracies. The modes can then be represented approximately (yet accurately) by so-called linearly polarized (LP) modes, which are a linear combination of the degenerate exact modes, chosen to be linearly polarized and nearly transverse [21]. The $\mathrm{LP}_{m,n}$ modes are composed of the following exact modes:

1) the doubly degenerate $\mathrm{LP}_{0,n}$ are formed by both $\mathrm{HE}_{1,n}$ modes;
2) the four-fold degenerate $\mathrm{LP}_{1,n}$ are formed by $\mathrm{TE}_{0,n}$, $\mathrm{TM}_{0,n}$ and both $\mathrm{HE}_{2,n}$ modes;
3) the four-fold degenerate $\mathrm{LP}_{m,n}$ $(m \geq 2)$ are formed by $\mathrm{HE}_{m+1,n}$ and $\mathrm{EH}_{m-1,n}$ modes.

Two fundamental differences between conventional and hollow-core fibers make the applicability of this hybrid-mode nomenclature to air-core fibers not *a priori* obvious. First, in a conventional fiber the core modes are true guided modes confined by total internal reflection, whereas in an air-core PBF they are leaky modes confined by photonic band gap effects. Second, the guiding region of a conventional fiber has a cylindrical symmetry $(\mathrm{C}_{\infty v})$, whereas a perfect PBF has a hexagonal symmetry (C_{6v}). This lower symmetry has important consequences on the modal characteristics of a PBF, since it would appear that its core modes cannot simply be described using a mode type (HE, EH, TE or TM) and two quantum numbers. For example, in a conventional fiber the H_z field of the HE_{1m} mode depends on azimuthal angle ϕ as exactly $\exp(-i\phi)$, but this dependency is not strictly correct in a PBF, since a PBF structure does not have exact rotational symmetry.

According to group theory, the modes of a waveguide with C_{6v} symmetry can be classified into six different irreducible representations, which specify four non-degenerate and two doubly degenerate mode classes [22], [23]. The non-degenerate modes reflect the full symmetry of the structure. The doubly degenerate modes do not exhibit the full symmetry of the structure. Rather, for any linear combination of a pair of doubly degenerate modes, any symmetry operation in C_{6v} transforms it into another linear combination of the same pair of doubly degenerate modes. It should be noted, however, that the mode degeneracies of a waveguide predicted by the irreducible representations of the waveguide symmetry occur at any arbitrary wavelength. The dispersion curves of two different modes of a waveguide, in general, may cross at some discrete points, thus creating some "accidental" degeneracy [23]. Such degeneracies cannot be predicted using the aforementioned mode classification based on the irreducible representations of the waveguide symmetry. In principle, the modes of a photonic-crystal fiber structure must be classified according to such irreducible representations.

One could, however, make connection between such classification based upon group theory, and the classifications derived from an analogy with conventional cylindrical fiber. For example, the TE_{0m} and TM_{0m} modes of a conventional cylindrical fiber belong to the A_2 and A_1 irreducible representation of the C_{6v} group, respectively, both of which are one-dimensional. In particular, irreducible representation A_1 is invariant under all the symmetry operations in C_{6v} group, while irreducible representation A_2 is rotationally invariant but anti-symmetrical under the mirror operations of C_{6v} group [22]. Conversely, therefore, the lowest order modes of an air-core fiber that belong to these two irreducible representations can be labeled TE_{0m} and TM_{0m} modes, respectively. Similarly, one can show that the HE_{1m} modes of a conventional cylindrical fiber belong to the E_1 irreducible representation of the C_{6v} group, which is two-dimensional. And hence we can label the lowest order doubly degenerate modes in this E_1 irreducible representation as HE_{1m} modes.

By analogy with cylindrical fiber, one might expect that hybrid modes like HE_{31} should also be doubly degenerate. However, we also know that when m is a multiple of three, hybrid modes like $\mathrm{HE}_{m,n}$ and $\mathrm{EH}_{m,n}$ exhibit C_{6v} symmetry. Therefore, in an air-core fiber these modes should not be degenerate. As we will show, these modes belong to the B_1 and B_2 irreducible representations of C_{6v} group, which are one-dimensional. This prediction is indeed supported by a study of the modes of a solid-core microstructured fiber with a hexagonal symmetry [19]. This same reference also demonstrated, as expected from similar symmetry arguments, that when the hole lattice in the cladding of this solid-core fiber is changed from hexagonal to square (C_{4v} symmetry), instead of the HE_{31} mode, it is the doubly degenerate HE_{21} mode that splits into two non-degenerate modes labeled HE_{211} and HE_{212} [19]. As we show in Section IV, in an air-core fiber with a C_{6v} symmetry the $\mathrm{HE}_{3n,m}$ modes split similarly into two non-degenerate modes.

As a point of comparison, it is useful to consider the special case of Bragg fibers [24], which also utilize a bandgap effect for guidance but have a higher symmetry than PBFs. In their ideal conceptual geometry, the core of a PBF consists of a cylinder of low-index material (possibly air) surrounded by concentric cylindrical layers of alternately high and low index [24]–[26]. Guidance in the core region relies on properly phased Bragg reflections off these multiple layers of high index contrast. Unlike a PBF, an ideal Bragg fiber has perfect cylindrical symmetry $(\mathrm{C}_{\infty v})$, and its guided modes are cylindrically symmetric. However, because of fabrication constraints practical Bragg fibers are not quite cylindrically symmetric, and consequently neither are their modes. In spite of this limitation, their symmetry class is still much closer to $\mathrm{C}_{\infty v}$ than hollow-core PBFs. The modes of practical Bragg fibers, albeit leaky as they are, are therefore still well described by the same hybrid modes (quasi-$\mathrm{TE}_{m,n}$, quasi-$\mathrm{TM}_{m,n}$, $\mathrm{HE}_{m,n}$, and $\mathrm{EH}_{m,n}$) as conventional fibers [25], [26].

TABLE I
THE IRREDUCIBLE REPRESENTATIONS OF THE MODES OF A PBF AND A CONVENTIONAL FIBER

Mode	Irreducible representation of C_{6v} symmetry group	Irreducible representation of $C_{\infty v}$ symmetry group
HE_{11}	E_1	E_1
HE_{21}	E_2	E_2
TE_{01}	A_2	A_2
TM_{01}	A_1	A_1
$HE_{31}^{(1)}$	B_1	E_3
$HE_{31}^{(2)}$	B_2	
EH_{11}	E_1	E_1
HE_{12}	E_1	E_1
HE_{41}	E_2	E_4
EH_{21}	E_2	E_2

Based on these considerations, one expects that because a PBF is only slightly less symmetric than an ideal Bragg or conventional fiber, it should also share the same nomenclature. To rigorously justify the proposed nomenclature, it is worth discussing briefly the main similarities and differences of the modes of these different fibers. A cylindrical fiber with $C_{\infty v}$ symmetry has two one-dimensional irreducible representations denoted A_1 and A_2, plus an infinite number of two-dimensional irreducible representations denoted E_n, where n is a positive integer. It can be shown simply that the TM_{0m} and TE_{0m} modes belong to A_1 and A_2, and the HE_{nm} and EH_{nm} modes belong to the E_n irreducible representations. The C_{6v} symmetry group, on the other hand, has four one-dimensional irreducible representations denoted A_1, A_2, B_1, and B_2, and two two-dimensional irreducible representations E_1 and E_2. The TM_{0m} and TE_{0m} modes belong to A_1 and A_2, the HE_{nm} and EH_{nm} modes belong to E_1 when n is odd and not a multiple of three, and they belong to E_2 when n is even and again not a multiple of three. As mentioned earlier, when n is a multiple of three, these hybrid modes split into two non-degenerate modes that belong to either B_1 or B_2. For clarity, we have summarized in Table I the irreducible representations to which the modes of a PBF and of a conventional fiber belong.

Although similar notations are utilized for C_{6v} and $C_{\infty v}$, it should be noted that the irreducible representations that share the same name do not necessarily have exactly the same characteristics. For example, as mentioned earlier, the TM_{0m} modes of a PBF with C_{6v} symmetry belong to A_1. This irreducible representation does not change if transformed by the $C_{\pi/6}$ symmetry operation (rotation by $\pi/6$). In contrast, the A_1 irreducible representation of $C_{\infty v}$ is unchanged by a rotation of any arbitrary angle. As will be shown, this difference becomes more evident for the HE_{nm} and EH_{nm} modes with $n > 2$. For example, the HE_{41} mode of a PBF (E_2 irreducible representation of C_{6v}) evidently looks different from the corresponding mode of a conventional fiber (E_4 irreducible representation of $C_{\infty v}$). A mode that belongs to the E_4 irreducible representation of $C_{\infty v}$ does not change if transformed by $C_{\pi/2}$, whereas a mode that belongs to the E_2 irreducible representation of C_{6v} does not change if transformed by C_{π}.

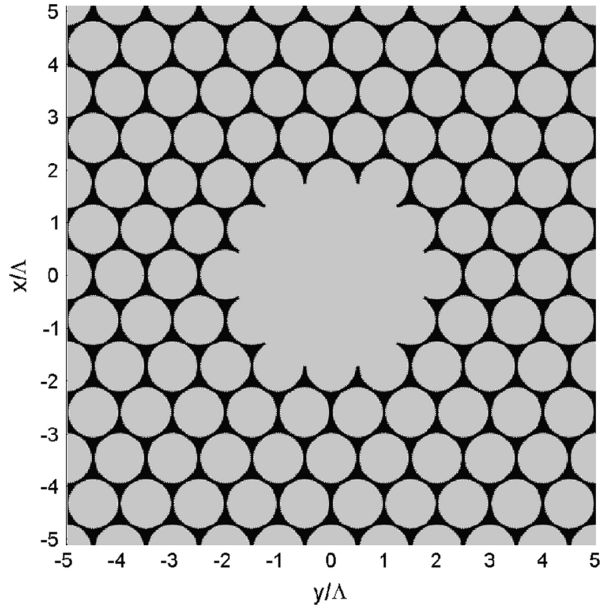

Fig. 1. Refractive index distribution of the modeled PBF. Gray areas represent air (refractive index 1), black areas represent silica (refractive index 1.45). The photonic crystal period is Λ; the cladding air hole radius is $\rho = 0.47\Lambda$, and the core radius is $R = 1.8\Lambda$.

To confirm the nature of these modes predicted by these group-theory arguments, in the following we compare the dispersion curves and field profiles of the modes of a slightly multimoded PBF with those of a conventional fiber. In spite of the aforementioned differences between these sets of modes, we show that there is a good qualitative agreement between their dispersion and profiles.

III. SIMULATION METHODOLOGY

To this end, we simulated the modal characteristics of a PBF with a core large enough to support a few higher order core modes, including the HE_{31} modes. The fiber we chose to model (Fig. 1) has the general characteristics of most of the hollow-core fibers studied to date, including commercial fibers. The cladding comprises a photonic crystal made of a two-dimensional periodic lattice of circular holes arranged in a triangular pattern of period Λ. This lattice is embedded in a matrix of homogeneous refractive index higher than the index of the holes. The core consists in a larger circular hole of radius R cut into the center of the photonic crystal and made of the same low-index material as the holes. Without loss of generality, we simulated the common case of holes filled with air $(\text{index} = 1)$ and of a matrix made of silica $(\text{index} = 1.45$ at a wavelength of 1.55 μm). The radius of cladding holes is $\rho = 0.47\Lambda$. The core radius was selected to be $R = 1.8\Lambda$ The reason for this choice is that this value falls in a range where the fiber does not support surface modes [11]. When surface modes are present, the core modes are generally perturbed, especially at wavelengths where a core-mode dispersion curve crosses a surface-mode dispersion curve [9], which might obscure some of the results of this analysis. Note that other than this special attention to suppressing unwanted surface modes, there is nothing particular about this set of parameters; any other selection would have yielded identical qualitative conclusions.

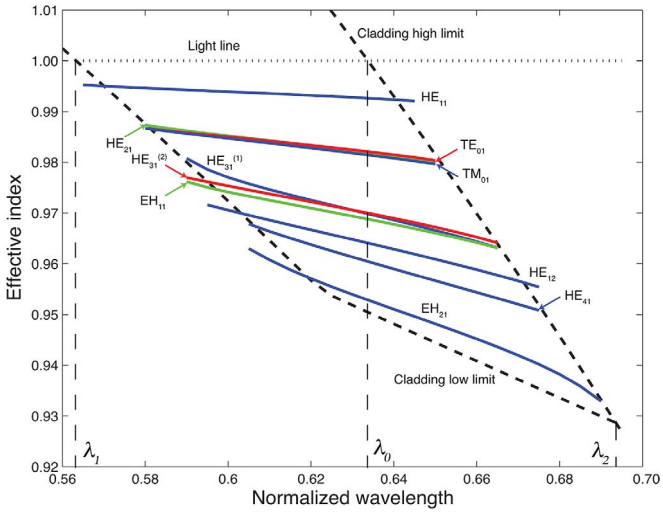

Fig. 2. Dispersion curve for all the core modes of the PBF shown in Fig. 1.

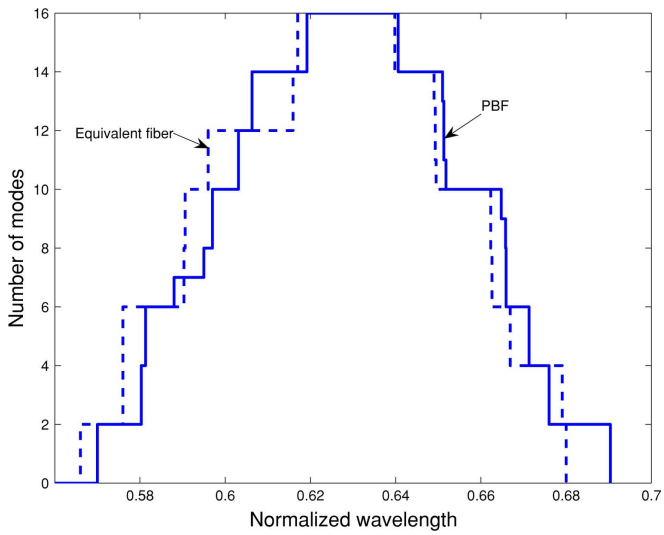

Fig. 3. Calculated number of core modes as a function of normalized wavelength for the PBF of Fig. 1 and for the equivalent step-index fiber.

The modes of this PBF were modeled using the SPBF code [18], a full-vectorial finite-difference mode solver utilizing a hexagonal Yee's cell, which has the same symmetry (C_{6v}) as the modeled fiber. As shown in [27], matching the cell symmetry to that of the fiber is essential to most accurately describe the modal properties and degeneracies of the fiber. To save computation memory, the PBF modes were computed over only in one quarter of a rhombus-shaped supercell, and the full modes were reconstructed over the entire supercell using their known individual symmetry. The side length of the supercell was 10Λ, and the spatial resolution was $\Lambda/72$, the maximum value that could be used with 3.2 gigabytes of available memory. This spatial resolution was adequate to obtain very good convergence of the calculated dispersion curves of the fiber over the entire bandgap.

IV. Simulation Results: Dispersion Curves

The calculated dispersion curves for all the core modes of this fiber are plotted in Fig. 2. The horizontal axis is the normalized wavelength λ/Λ. The two dashed black curves represent the cladding's upper and lower bands, and the dotted curve is the light line (it should be noted that frequency band edges are used throughout the paper). The bandgap extends from a wavelength of $\lambda = 0.56\Lambda$ to 0.70Λ. Each dispersion curve is labeled with the core mode corresponding to it, according to the nomenclature proposed and discussed in Section V.

Unlike in conventional fibers, the core modes exhibit both a short-wavelength and a long-wavelength cutoff. As a result, unlike in a conventional or solid-core microstructured fiber, the dependence of the number of core modes on frequency is not monotonic. This dependence, taken directly from Fig. 2, is made more explicit in Fig. 3 (solid curve). As the wavelength is increased from the short-wavelength cutoff of the lowest order mode ($\lambda = \lambda_1 = 0.56\Lambda$), the number of modes increases from zero, usually in increments of 2, and occasionally in increments of 1 in the vicinity of some cutoff wavelengths. It eventually reaches a maximum of 16 modes at $\lambda = 0.62\Lambda$, and remains at this maximum up to $\lambda = \lambda_0 = 0.64\Lambda$, where λ_0 is the wavelength where the lower band edge intersects the light line. Above λ_0, the number of modes decreases, in the same increments of 1 or 2, until it reaches zero at $\lambda = \lambda_2 = 0.70\Lambda$.

This behavior is well explained by the geometrical-optics interpretation developed in [17]. Since this interpretation is critical for the rest of this paper, we briefly summarize its highlights in the rest of this section. To be a core mode, with reference to Fig. 2 as an example, a mode must have its effective index below the light line, below the lower band edge, and above the upper band edge. The modal properties of a PBF can therefore be assimilated to the properties of an equivalent conventional fiber whose index profile is defined in such a way that these three conditions are met. The first condition (no core mode can propagate above the light line) imposes that the core index of the equivalent fiber is simply $n_1 = 1$, at all wavelengths. The second condition (no core mode can propagate below the upper band edge) imposes that the cladding must have an index $n_2 = k_U(\lambda)/k_0$, where $k_U(\lambda)$ is the k_z of the upper band edge and $k_0 = 2\pi/\lambda$ is the wave-number at λ. n_2 is therefore a function of wavelength [17]. So at the short-wavelength edge of the bandgap (λ_1), where the light line intersects the upper band edge (see Fig. 2), $n_2 = n_1$, hence $\mathrm{NA} = 0$ and the fiber supports no core modes, as can be seen in Fig. 3. Above λ_1, the NA increases monotonically, reaching its maximum at the long-wavelength edge of the bandgap (λ_2), where the upper and lower band edges cross. The third condition (no mode can propagate above the lower band edge) implies that for wavelengths above λ_0 (see Fig. 2), of the core modes supported by the equivalent fiber (defined by a core index $n_1 = 1$ and a cladding index $n_2(\lambda)$), the only modes allowed are the ones with an effective index lower than $n_3 = k_L(\lambda)/k_0$, where $k_L(\lambda)$ is the k_z of the lower band edge [17]. This condition can be easily expressed by introducing a second cladding index n_3 (or equivalently a second numerical aperture) *above* which all modes are cutoff [17]. It means that as the wavelength is increased above λ_0, the first numerical aperture remains the same but the second one increases, i.e., the effective NA of the fiber decreases. The lower order modes are gradually cut off, until all modes are cut off at

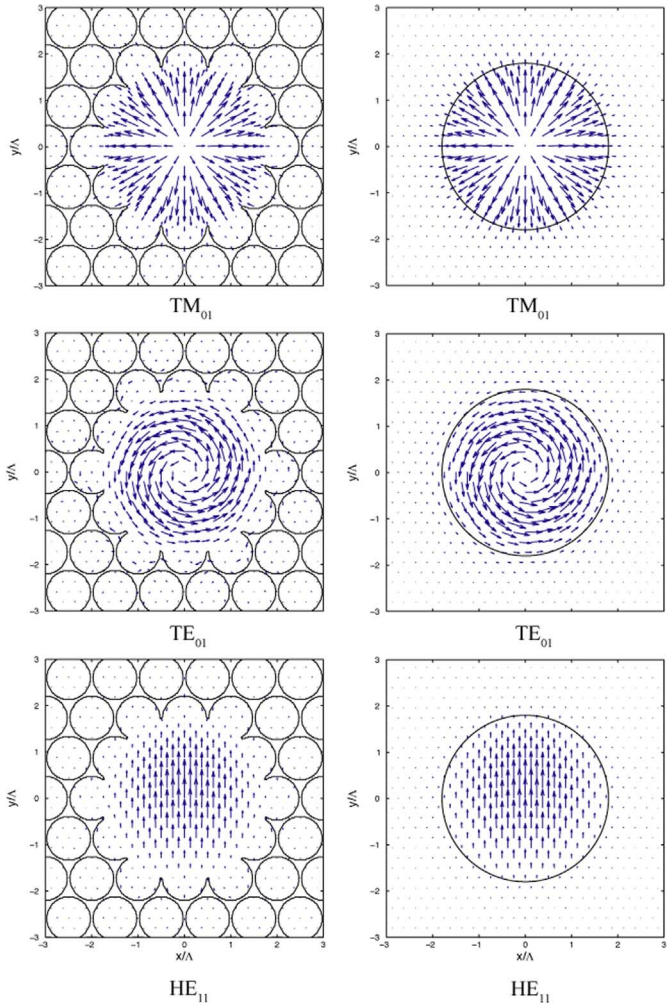

Fig. 4. Calculated transverse electric field of selected modes of the PBF of Fig. 1 (left column) and of the equivalent step-index fiber (right column) at $\lambda = 0.64\Lambda$.

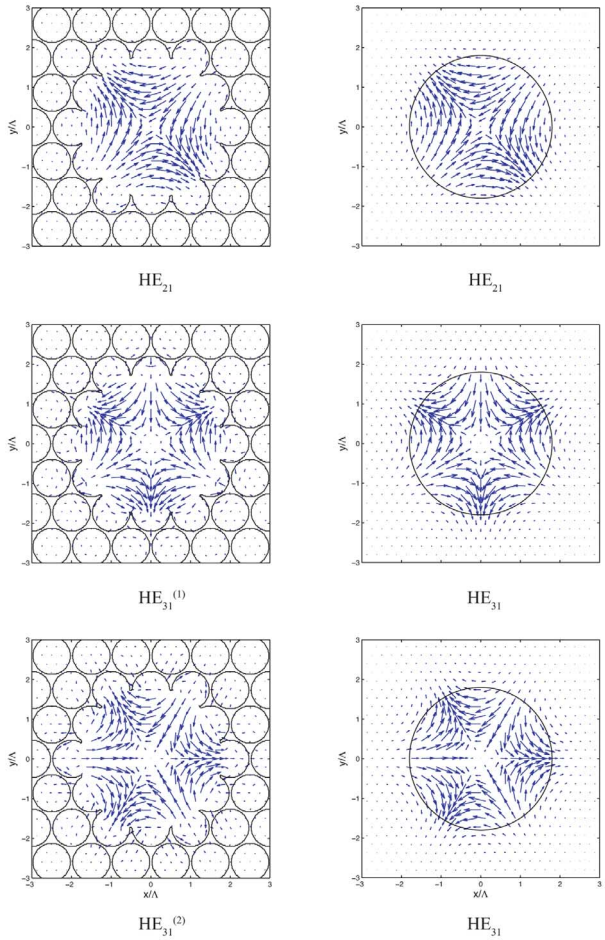

Fig. 4. *(continued)* Calculated transverse electric field of selected modes of the PBF of Fig. 1 (left column) and of the equivalent step-index fiber (right column) at $\lambda = 0.64\Lambda$.

λ_2, in agreement with Fig. 3. If, furthermore, the equivalent fiber is defined as having a core radius equal to the core radius of the PBF, it was shown in [17] that the core modes of the PBF exhibit similar qualitative behavior as the $\mathrm{LP}_{n,m}$ modes of this equivalent step-index fiber. We refer the reader to [17] for a more detailed description of this analogy.

To illustrate this equivalence, we also plotted in Fig. 3 (dashed curve) the evolution of the number of modes as a function of normalized wavelength for the equivalent step-index fiber. This curve was generated by: 1) calculating from the bandgap diagram, at each wavelength, the two NAs of the equivalent fiber, 2) calculating the modes of this conventional fiber, and 3) plotting the number of modes versus wavelength. The dependence of the total number of modes on wavelength in a PBF clearly follows the same pattern as that of a conventional fiber. With the exception of certain groups of modes, discussed below, the number of modes jumps up or down in unison, the modes have similar cutoff wavelengths, and the maximum number of modes is the same.

Given the striking analogies between a PBF and a step-index fiber, it was interesting to investigate whether the LP-mode approximation and nomenclature are applicable for PBFs at frequencies where the PBF's equivalent NA is low. Reference to the dispersion diagram (Fig. 2) shows that even at $\lambda = 0.58\Lambda$, where the equivalent NA is 0.157, the spread in the effective indices of the first four high order modes (HE_{21}, TE_{01}, and TM_{01}) is fairly large, and quite a bit larger than it is in the equivalent conventional fiber (6.3×10^{-4} versus 3.5×10^{-5}). Consequently, even at this small NA, the actual modes are not degenerate enough to be accurately represented by the four degenerate LP_{11} modes. Therefore, the LP approximation is not adequate to represent the modes of a PBF.

V. Mode Electric-Field Profiles and Nomenclature

The transverse electric field profiles of 10 of the PBF's core modes, calculated at a wavelength of $\lambda = 0.64\Lambda$ where the PBF supports its maximum number of modes, are plotted in Fig. 4. These ten modes were chosen such that each of the groups of degenerate or non-degenerate modes is represented. For identification and comparison purposes, these profiles are shown side by side with the profiles of the modes of the equivalent fiber, defined according to the criteria outlined in the previous section. This equivalent fiber therefore has a core radius equal to that of the PBF ($R = 1.8\Lambda$), a core index $n_1 = 1$, and, at this wavelength, a cladding index $n_2 = 0.948$ ($\mathrm{NA} = 0.318$). We also

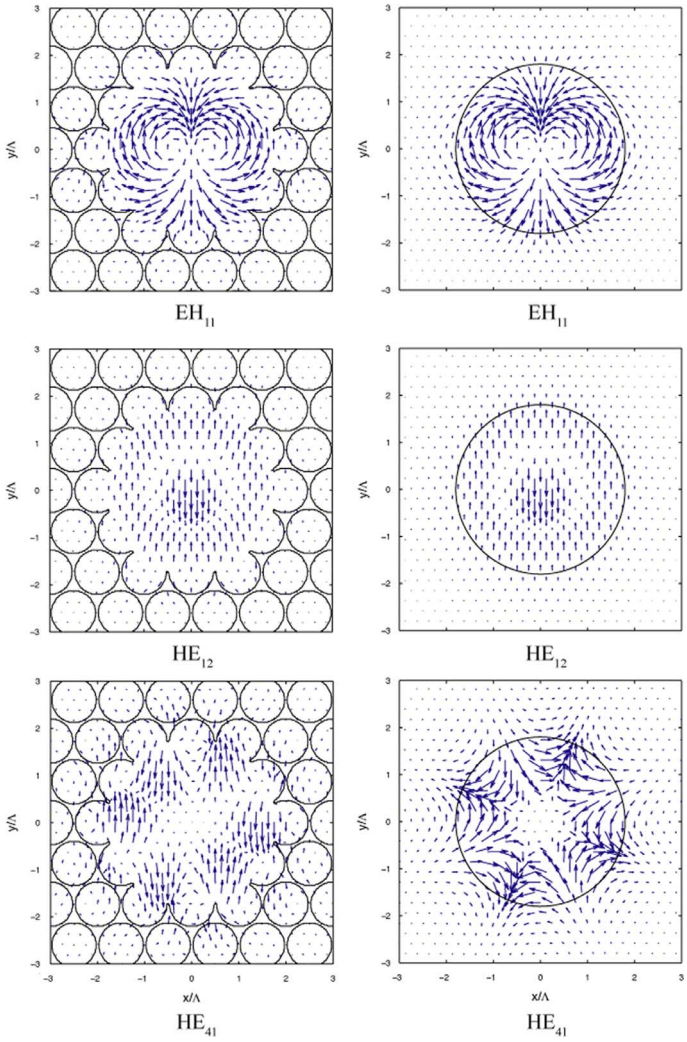

Fig. 4. *(continued)* Calculated transverse electric field of selected modes of the PBF of Fig. 1 (left column) and of the equivalent step-index fiber (right column) at $\lambda = 0.64\Lambda$.

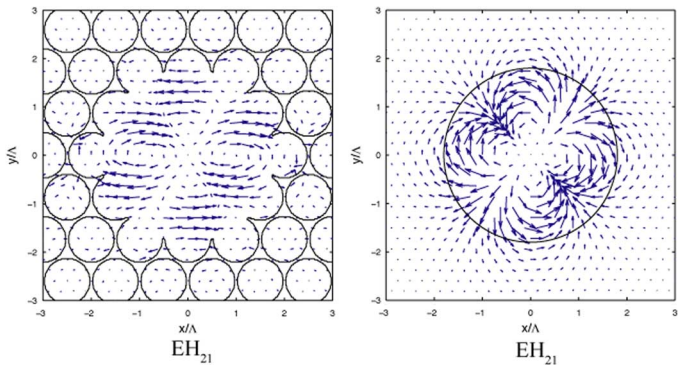

Fig. 4. *(continued)* Calculated transverse electric field of selected modes of the PBF of Fig. 1 (left column) and of the equivalent step-index fiber (right column) at $\lambda = 0.64\Lambda$.

show in Fig. 5 the intensity profiles (Poynting vector distributions) of these same modes.

In almost all cases, we observe extremely similar features in the conventional fiber mode and the corresponding PBF mode,

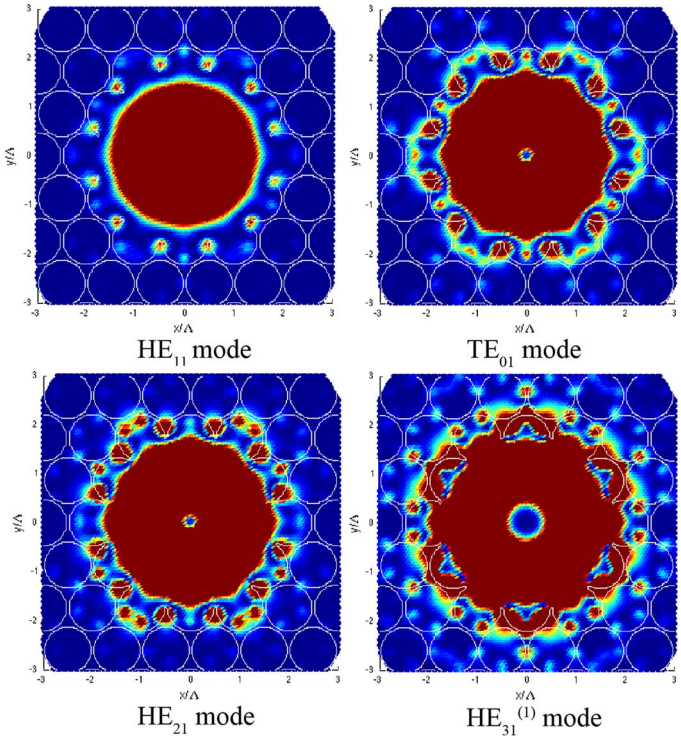

Fig. 5. Comparison of the intensity profile of selected core modes of the PBF of Fig. 1, calculated at $\lambda = 0.64\Lambda$.

both in terms of radial and azimuthal distributions and symmetries. Most of the differences between fiber and PBF modes are small and confined to the PBF core-cladding boundary region. They are caused by the scalloped shape of the PBF core and the presence in this vicinity of high-index membranes, as opposed to the smooth circular shape of the conventional fiber core. As is well known, these high-index regions act as local field concentrators and result in weak local out-of-phase side lobes where the mode is locally guided by these regions.

The only PBF modes that clearly deviate from the ones of the equivalent conventional fiber are the highest order modes HE_{41} and EH_{21}. These differences were expected from our group theory arguments of Section II. Specifically, the EH_{21} mode belongs to the E_2 irreducible representation of $\mathrm{C}_{\infty v}$ for the conventional fiber, and the C_{6v} for the PBF. However, as pointed out earlier these two E_2 representations have different characteristics. For example, the $\mathrm{C}_{\pi/2}$ symmetry operation transforms the E_2 irreducible representation of $\mathrm{C}_{\infty v}$ to the minus of this representation. However, the $\mathrm{C}_{\pi/2}$ operation (i.e., a 90-degree rotation) does not belong to the C_{6v} group. Hence, the EH_{21} mode in the air-core fiber differs in its modal profile substantially from the EH_{21} mode in the conventional fiber. The same argument can also be applied to HE_{21} mode. The difference is slight, and not readily apparent in Fig. 4. However, close inspection of the intensity profile of this mode (Fig. 5) reveals that the $\mathrm{C}_{\pi/2}$ operation does not transform it to minus itself. Specifically, this mode has a profile that is elongated in the horizontal direction. Using similar arguments, we expect that in general the deviation in modal profile between a PBF mode and its equivalent conventional fiber mode will become more evident as the order of the mode increases. Specifically, such deviation should

TABLE II
COMPARISON OF THE MODE ORDER IN THE PBF UNDER STUDY AND EQUIVALENT CONVENTIONAL FIBER

PBF modes short-wavelength cutoff		HE_{11}	HE_{21}	quasi-TE_{01}	quasi-TM_{01}	$HE_{31}^{(1)}$	$HE_{31}^{(2)}$	EH_{11}	HE_{12}	HE_{41}	EH_{21}
PBF modes long-wavelength cutoff		HE_{11}	quasi-TE_{01}	HE_{21}	quasi-TM_{01}	$HE_{31}^{(2)}$	$HE_{31}^{(1)}$	EH_{11}	HE_{12}	HE_{41}	EH_{21}
Conventional fiber	**Hybrid modes**	HE_{11}	TE_{01}	HE_{21}	TM_{01}	EH_{11}	HE_{31}		HE_{12}	EH_{21}	HE_{41}
	LP modes	LP_{01}	LP_{11}			LP_{21}			LP_{02}	LP_{31}	

TABLE III
DEGENERACY OF THE CORE MODES OF THE PBF UNDER STUDY

PBF modes	HE_{11}	HE_{21}	quasi-TE_{01}	quasi-TM_{01}	$HE_{31}^{(1)}$	$HE_{31}^{(2)}$	EH_{11}	HE_{12}	HE_{41}	EH_{21}
Mode degeneracy	2	2	1	1	1	1	2	2	2	2

occur for conventional modes that do not have C_{6v} symmetry, as demonstrated by the EH_{21} mode, for example, in the foregoing analysis. On the other hand, it should not occur for the higher order modes with C_{6v} symmetry, as demonstrated by the HE_{3m} modes, for example. These predictions are supported by all the higher order modes of the PBF we investigated. We also found that it applied to all the modes of an even more multimoded fiber (a fiber with a core radius $R = 2.7\Lambda$), not shown here for conciseness.

Applying this comparison process to all the other modes of the PBF at this wavelength enabled us to identify all of them and label them as shown in Fig. 2. All modes are observed to be either hybrid (comparable to conventional HE/EH fiber modes) or quasi-transverse (comparable to conventional TE/TM fiber modes). The quasi-transverse nature of the latter group of modes is due to the fiber's weaker symmetry (C_{6v}), as opposed to the $C_{\infty v}$ symmetry of a conventional fiber, which ensures complete transversality of some of its modes. Furthermore, all of the PBF core modes exhibit radial and azimuthal nodes consistent with the traditional use of the radial and azimuthal mode numbers in conventional fibers.

Based on the foregoing, we suggest the adoption of the same hybrid-mode classification to label the modes of a PBF as used in conventional fibers, namely $HE_{m,n}$, $EH_{m,n}$, quasi-$TE_{0,n}$, or quasi-$TM_{0,n}$. This result is non-obvious considering the nature of the respective waveguide symmetries and the major physical differences in their guiding mechanisms. The only exception to this hybrid mode nomenclature compared to a conventional fiber is the $HE_{3p,n}$ and $EH_{3p,n}$ modes, where p is an integer. These modes, which are degenerate in a waveguide with cylindrical symmetry $(C_{\infty v})$, split into two non-degenerate modes each in a waveguide with a C_{6v} symmetry. This is well illustrated for the two HE_{31} modes in the dispersion diagram of the fiber under study (Fig. 2), which are non-degenerate across all of the bandgap, except for the wavelength where their dispersion curves cross ($\lambda \approx 0.63\Lambda$). To differentiate these now distinct hybrid modes from each other, we have labeled them $HE_{31}^{(1)}$ and $HE_{31}^{(2)}$. This difference is entirely analogous to the splitting of the HE_{31} modes pointed out in [19] in the case of a microstructured fiber with a C_{6v} symmetry.

VI. CUTOFF WAVELENGTHS AND DEGENERACIES

In the light of this nomenclature and analogy with conventional fibers, the modes dispersion curves (Fig. 2) yield further useful analogy, as well as subtle differences, between the hybrid modes of the two types of fiber. First, the relative position of the *groups* of modes in the effective index space is exactly the same as for an index-guided fiber. Specifically, the modes with the highest effective index are the two degenerate HE_{11} modes, followed by the $\{HE_{21}, \text{quasi-}TE_{01}, \text{quasi-}TM_{01}\}$ group of modes (which would be LP_{11} modes in a weakly guiding fiber), the $\{HE_{31}, EH_{11}\}$ group (LP_{21} mode), the HE_{12} mode, and finally the $\{HE_{41}, EH_{21}\}$ group (LP_{31} mode). In other words, the groups of modes cut off (in the traditional sense of long-wavelength cutoff) in the same order as the groups of modes of a conventional fiber.

Second, within each of the two groups of modes that are not made purely of two-fold degenerate modes, namely the $\{HE_{21}, \text{quasi-}TE_{01}, \text{quasi-}TM_{01}\}$ and $\{HE_{31}, EH_{11}\}$ groups, the high and the low cutoff wavelengths do not occur in the same order. The reason is that some of the dispersion curves cross, whereas they do not in the equivalent index-guided fiber. For example, Fig. 2 shows that in the first of the aforementioned groups, the HE_{21} mode appears first, followed by the quasi-TE_{01} and quasi-TM_{01} modes (which appear simultaneously), but at long wavelength the modes cut off in a different order, namely, quasi-TE_{01}, HE_{21}, and quasi-TM_{01}. Note that for the third group ($\{HE_{41}, EH_{21}\}$), the high and the low cutoff wavelengths *do* occur in the same order, but this order is reversed from what it is in the equivalent step-index fiber.

Table II summarizes these parallels and differences by listing the order in which the modes of the PBF under study are cut off (both the short and long cutoff wavelengths), as well as the order in which the modes of the equivalent index-guided fiber are cut off (again in the traditional, long-wavelength sense). For reference, the table also shows the order of appearance of the LP modes of a step-index fiber. This comparison shows clearly that the order of the long-wavelength cutoffs are the same for all modes except for the HE_{31} and EH_{11} modes, which occur in reverse order. The order of the long-wavelength cutoffs is also the

same for the first four modes (HE_{11}, quasi-TE_{01}, HE_{21}, and quasi-TM_{01}) and the HE_{12} modes, but the order of the HE_{31} and EH_{11} modes are reversed, and so it is for the HE_{41} and EH_{21} modes. This reversal is particularly pronounced for these last two modes, and the gap between them is much larger than in the equivalent step-index fiber. As mentioned in the last section, since the HE_{41} and EH_{21} modes of the PBF do not have exactly the same characteristics as the corresponding modes of its equivalent step-index fiber, one should not expect similar dispersion characteristics for these modes. It should, however, be noted that the order of the mode cut-offs presented in Table II is particular to the studied PBF. The location of the crossing points between the modes of a given group, and therefore the order of mode cut-offs, in general, depends on the geometry of the PBF. Note also that the degeneracy of all the core modes of the PBF, listed in Table III, are identical to the mode degeneracy in a conventional fiber, with the above noted exception that the HE_{31} modes are split in a PBF.

As mentioned in Section III, the core radius of the PBF studied in this paper was selected to avoid surface modes. When the fiber supports surface modes, the core modes are generally perturbed by these modes. The perturbation is very strong where the surface modes cross the dispersion curves of the core modes of the fiber. This may affect some of our results, for example, the short- and long-wavelength cutoffs. However, we expect that our arguments about the similarities and the differences in the modes of a PBF and those of its equivalent conventional fiber are valid, at least, where the modes are not strongly perturbed by surface modes.

In addition, note that C_{6v} symmetry alone does not guarantee that the modes will have modal profiles similar to those of a conventional fiber. Thus, in principle, one needs to examine the structures on a case-by-case basis in order to see how well the analogy to conventional fiber holds. However, we expect that our results apply to a large number of photonic bandgap fibers. Since most of the lower order modes in a photonic-bandgap fiber have smooth enough field variation, these modes can be approximated by conventional fiber modes.

VII. Conclusion

By studying the dispersion curves, field profiles, and cutoff wavelengths of a slightly multimoded (16 modes) air-core photonic-bandgap fiber, we have established that despite their major differences in symmetry and guiding mechanism, PBFs and conventional fibers exhibit strikingly similar modal behavior, down to fine details. Specifically, except for the $HE_{3n,m}$ and $EH_{3n,m}$ modes, the groups of higher order modes of a PBF appear in the same order as the groups of hybrid modes of a conventional index-guiding fiber, and they exhibit the same degeneracies. Furthermore, their intensity profiles exhibit strong similarities, except for the HE_{21}, EH_{21}, and HE_{41} modes. These deviations are generally expected from group theory arguments for the HE_{nm} and EH_{nm} modes when n is larger than one. These similarities suggest that the hybrid mode classification used in conventional fibers is applicable to PBFs, provided the transverse modes be labeled quasi-transverse to account for their small but finite longitudinal field component.

References

[1] D. G. Ouzounov, F. R. Ahmad, A. L. Gaeta, D. Müller, N. Venkataraman, M. T. Gallagher, and K. W. Koch, "Dispersion and nonlinear propagation in air-core photonic band-gap fibers," in *Conf. Lasers and Electro-Optics*, Baltimore, MD, 2003.

[2] V. Dangui, H. K. Kim, M. J. F. Digonnet, and G. S. Kino, "Phase sensitivity to temperature of the fundamental mode in air-guiding photonic-bandgap fibers," *Opt. Express*, vol. 13, no. 18, pp. 6669–6684, 2005.

[3] S. Blin, H. K. Kim, M. J. F. Digonnet, and G. S. Kino, "Reduced thermal sensitivity of a fiber-optic gyroscope using an air-core photonic-bandgap fiber," *J. Lightw. Technol.*, vol. 25, no. 3, pp. 861–865, Mar. 2007.

[4] J. Tauer, F. Orban, H. Kofler, A. B. Fedotov, and I. V. Fedotov, "High-throughput of single high-power laser pulses by hollow photonic band gap fibers," *Laser Phys. Lett.*, vol. 4, no. 6, pp. 444–448, June 2007.

[5] D. G. Ouzounov, F. R. Ahmad, D. Müller, N. Venkataraman, M. T. Gallagher, M. G. Thomas, J. Silcox, K. W. Koch, and A. L. Gaeta, "Generation of megawatt optical solitons in hollow-core photonic band-gap fibers," *Science*, vol. 301, pp. 1702–1704, Sep. 2003.

[6] D. G. Ouzounov, C. J. Hensley, A. L. Gaeta, N. Venkataraman, M. T. Gallagher, and K. W. Koch, "Soliton pulse compression in photonic bandgap fibers," *Opt. Express*, vol. 13, no. 16, pp. 6153–6159, 2005.

[7] K. Mukasa, F. Poletti, M. Petrovich, N. Broderick, R. Amezcua-Correa, M. A. F. Roelens, and D. J. Richardson, "Possible future applications of photonic bandgap fiber in non-repeatered transmission systems," in *Opt. Fiber Commun. Conf.*, Anaheim, CA, 2007, paper OML1.

[8] H. K. Kim, V. Dangui, M. J. F. Digonnet, and G. S. Kino, "Fiber-optic gyroscope using an air-core fiber," in *SPIE Proc.*, 2005, vol. 5855, pp. 198–201.

[9] J. A. West, C. M. Smith, N. F. Borrelli, D. C. Allan, and K. W. Koch, "Surface modes in air-core photonic band-gap fibers," *Opt. Express*, vol. 12, no. 8, pp. 1485–1496, Apr. 2004.

[10] R. Amezcua-Correa, F. Gèrôme, S. G. Leon-Saval, N. G. R. Broderick, T. A. Birks, and J. C. Knight, "Control of surface modes in low loss hollow-core photonic bandgap fibers," *Opt. Express*, vol. 16, no. 2, pp. 1142–1149, Jan. 2008.

[11] H. K. Kim, J. Shin, S. Fan, M. J. F. Digonnet, and G. S. Kino, "Designing air-core photonic-bandgap fibers free of surface modes," *J. Quantum Electron.*, vol. 40, no. 5, pp. 551–556, May 2004.

[12] K. Saitoh, N. J. Florous, T. Murao, and M. Koshiba, "Design of photonic band gap fibers with suppressed higher order modes: Towards the development of effectively single mode large hollow-core fiber platforms," *Opt. Express*, vol. 14, no. 16, pp. 7342–7352, Jul. 2006.

[13] M. Petrovich, F. Poletti, A. van Brakel, and D. J. Richardson, "Robustly single mode hollow core photonic bandgap fiber," *Opt. Express*, vol. 16, no. 16, pp. 4337–4346, 2008.

[14] P. J. Roberts, J. Broeng, A. Petersson, and K. P. Hansen, "Amplification in hollow core photonic crystal fibers," in *Fiber Lasers III: Technology, Systems, and Applications, Proc. SPIE*, 2006, vol. 6102, pp. 61020F-1–61020F-11.

[15] Y. Jeong, S. Baek, B. Lee, S. Choi, and K. Oh, "Macrobend sensor via the use of a hollow-core splice fiber: Theory and experiments," *Opt. Eng.*, vol. 4, no. 8, pp. 1815–1820, Aug. 2002.

[16] G. Vienne, Y. Xu, C. Jakobsen, H. J. Deyerl, J. Jenseon, T. Sorensen, T. Hansen, Y. Huang, M. Terrel, R. Lee, N. Mortensen, J. Broeng, H. Simonsen, A. Bjarklev, and A. Yariv, "Ultra-large bandwidth hollow-core guiding in all-silica Bragg fibers with nano-supports," *Opt. Express*, vol. 12, no. 15, pp. 3500–3508, Jul. 2004.

[17] M. J. F. Digonnet, H. K. Kim, G. S. Kino, and S. Fan, "Understanding air-core photonic-bandgap fibers: Analogy to conventional fibers," *J. Lightw. Technol.*, vol. 23, pp. 4169–4177, 2005.

[18] V. Dangui, M. J. F. Digonnet, and G. S. Kino, "A fast and accurate numerical tool to model the modal properties of photonic-bandgap fibers," *Opt. Express*, vol. 14, no. 7, pp. 2979–2993, 2006.

[19] R. Guobin, W. Zhi, L. Shuqin, and J. Shuisheng, "Mode classification and degeneracy in photonic crystal fibers," *Opt. Express*, vol. 11, no. 11, pp. 1310–1321, June 2003.

[20] D. Marcuse, *Theory of Dielectric Optical Waveguides*. New York: Academic Press, 1974, ch. 2.

[21] D. Gloge, "Weakly guiding fibers," *Appl. Opt.*, vol. 10, no. 10, pp. 2252–2258, Oct. 1971.

[22] M. Hamermesh, *Group Theory and Its Applications to Physical Problems*. New York: Dover, 1989, ch. 4.

[23] P. McIsaac, "Symmetry-induced modal characteristics of uniform waveguides I: Summary of results," *IEEE Trans. Microw. Theory Tech.*, vol. MTT-23, no. 5, pp. 421–429, 1975.

[24] P. Yeh, A. Yariv, and E. Marom, "Theory of Bragg fiber," *J. Opt. Soc. Am.*, vol. 68, no. 9, pp. 1196–1201, Sep. 1978.

[25] A. Argyros, "Guided modes and loss of Bragg fibres," *Opt. Express*, vol. 10, no. 24, pp. 1411–1417, Nov. 2002.
[26] Y. Xu, A. Yariv, J. G. Fleming, and S. Lin, "Asymptotic analysis of silicon based Bragg fibers," *Opt. Express*, vol. 11, no. 9, pp. 1039–1049, Apr. 2003.
[27] J. M. Fini, "Improved symmetry analysis of many-moded microstructure optical fibers," *J. Opt. Soc. Am. B*, vol. 21, no. 8, pp. 1431–1436, 2004.

Kiarash Zamani Aghaie received the B.S. and M.S. degrees in electrical engineering from the University of Tehran, Tehran, Iran, in 2002 and 2005, respectively.

His research interests include numerical modeling of photonic-bandgap fibers and photonic crystals, and photonic-bandgap fiber components.

Vinayak Dangui received the Diplome d'Ingenieur degree from Ecole Polytechnique, Paris, France, in 2000, and the M.S. and Ph.D. degrees in electrical engineering from Stanford University, Stanford, CA, in 2002 and 2008, respectively.

He is currently a Member of the Technical Staff at Infinera Corporation, Sunnyvale, CA. His previous research interests include semiconductor lasers, wireless digital communications and peer-to-peer networks. His current research interests include fiber optic communications, the modeling of photonic-bandgap fibers and photonic crystals, photonic-bandgap fiber components, and fiber optic sensors.

Michel J. F. Digonnet received the degree of engineering from Ecole Supérieure de Physique et de Chimie de la Ville de Paris, the Diplome d'Etudes Approfondies in coherent optics from the University of Paris, Orsay, France, in 1978, and the M.S. and Ph.D. degrees from the Applied Physics Department of Stanford University, Stanford, CA, in 1980 and 1983, respectively. His doctoral research centered on WDM fiber couplers and fiber lasers and amplifiers.

From 1983 to 1986, he was employed by Litton Guidance and Control, Chatsworth, CA, as a Visiting Scholar at Stanford, conducting research in miniature solid-state sources and integrated optics for fiber sensors. From 1986 to 1990, he was involved in the development of dye and 2-μm solid-state lasers, fiber sensors and delivery systems for laser angioplasty at MCM Laboratories, Mountain View, CA. Since then, he has been a Senior Research Associate in Stanford University's Applied Physics Department. His current interests include photonic-bandgap fibers, fiber sensor arrays, slow light in sensors, and fiber-based MEMS sensors. He has published 230 articles, holds 75 patents, edited several books, and chaired numerous conferences on optical fiber devices and fiber sensors. He teaches courses on fiber amplifiers, lasers, and fiber sensors.

Shanhui Fan (SM'06) was an undergraduate student in physics at the University of Science and Technology of China, Hefei, Anhui, China, from 1988 to 1992, and received the Ph.D. degree in physics from the Massachusetts Institute of Technology (MIT), Cambridge, in 1997. He was a Postdoctoral Research Associate in physics at MIT from 1997 to 1999 and a Research Scientist at the Research Laboratory of Electronics, MIT, from 1999 to 2001.

He is an Associate Professor of electrical engineering at Stanford University, Stanford, CA. He has been with Stanford University since 2001. His interests include theory and simulations of photonic and solid-state materials and devices, photonic crystals, nanoscale photonic devices and plasmonics, quantum optics, computational electromagnetics, and parallel scientific computing. He has published over 140 journal articles, has given more than 100 invited talks, and holds 28 U.S. patents.

Dr. Fan received the Adolph Lomb Medal from the Optical Society of America, the National Academy of Sciences Award for Initiative in Research, a David and Lucile Packard Fellowship, and a National Science Foundation Career Award. He is a Fellow of OSA, a senior member of IEEE, and a member of APS and SPIE.

Gordon S. Kino (LF'94) is the W. M. Keck Foundation Professor of Electrical Engineering, Emeritus, and Professor, by Courtesy, of Applied Physics, Emeritus. He was the Director of the E. L. Ginzton Laboratory at Stanford University, and Associate Dean of Engineering for Planning and Facilities. He received the B.Sc. and M.Sc. degrees in mathematics from London University, London, U.K., and the Ph.D. degree in electrical engineering from Stanford University, Stanford, CA.

He has worked on microwave tubes, electron guns, plasmas, the Gunn effect, acoustic devices, acoustic imaging, nondestructive testing, fiber-optics and optical and acoustic microscopy. His current interests are in fiber optic acoustic sensor arrays and miniature scanning optical microscopes for medical applications in endoscopes. He has published over 450 papers and has 50 patents. He and his students have developed new types of scanning optical microscopes and interferometric microscopes, and fiber optic acoustic sensor arrays, and invented the Real-Time Scanning Confocal Optical Microscope, the Mirau Correlation Microscope, the Solid Immersion Lens for optical microscopy and storage and a Micromachined Confocal Scanning Optical Microscope. With Timothy Corle, he authored *Confocal Optical Microscopy and Related Techniques* (Academic Press, 1996), and he is the author of *Acoustic Waves: Devices, Imaging, and Analog Signal Processing* (Prentice-Hall, Inc., 1987).

Dr. Kino was a Guggenheim Fellow in 1967 and is currently a Fellow of the IEEE, the American Physical Society, and the AAAS, and a member of the National Academy of Engineering. In 1984 he received the IEEE Ultrasonics Group Achievement Award and in 1986 the ASNT Achievement Award in Applied Research.